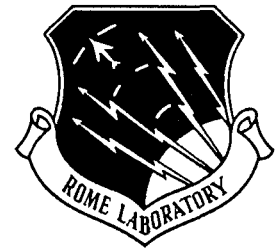
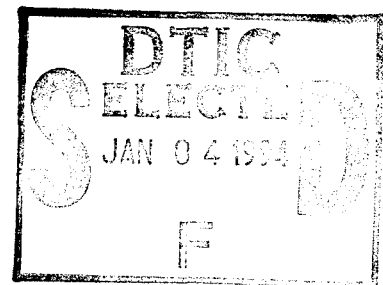


RL-TR-94-194
Final Technical Report
October 1994



DIGITAL OPTICAL COMPUTING



Alabama A&M University

S. Kupiec and H.J. Caulfield

DTIC QUALITY INSPECTED 2

APPROVED FOR PUBLIC RELEASE; DISTRIBUTION UNLIMITED.

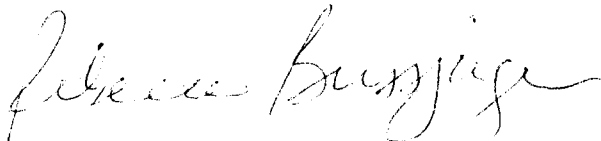
19941229 039

**Rome Laboratory
Air Force Materiel Command
Griffiss Air Force Base, New York**

This report has been reviewed by the Rome Laboratory Public Affairs Office (PA) and is releasable to the National Technical Information Service (NTIS). At NTIS it will be releasable to the general public, including foreign nations.

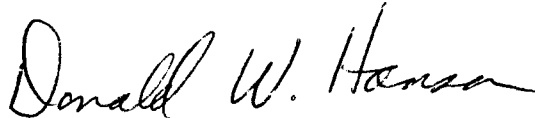
RL-TR-94-194 has been reviewed and is approved for publication.

APPROVED:



REBECCA BUSSJAGER
Project Engineer

FOR THE COMMANDER:



DONALD W. HANSON
Director of Surveillance & Photonics

If your address has changed or if you wish to be removed from the Rome Laboratory mailing list, or if the addressee is no longer employed by your organization, please notify RL (OCPB) Griffiss AFB NY 13441. This will assist us in maintaining a current mailing list.

Do not return copies of this report unless contractual obligations or notices on a specific document require that it be returned.

REPORT DOCUMENTATION PAGE

Form Approved
OMB No. 0704-0188

Public reporting burden for this collection of information is estimated to average 1 hour per response, including the time for reviewing instructions, searching existing data sources, gathering and maintaining the data needed, and completing and reviewing the collection of information. Send comments regarding this burden estimate or any other aspect of this collection of information, including suggestions for reducing this burden, to Washington Headquarters Services, Directorate for Information Operations and Reports, 1215 Jefferson Davis Highway, Suite 1204, Arlington, VA 22202-4302, and to the Office of Management and Budget, Paperwork Reduction Project (0704-0188), Washington, DC 20503.

1. AGENCY USE ONLY (Leave Blank)		2. REPORT DATE October 1994		3. REPORT TYPE AND DATES COVERED Final ----	
4. TITLE AND SUBTITLE DIGITAL OPTICAL COMPUTING				5. FUNDING NUMBERS C - F30602-92-C-0075 PE - 62702F PR - 4600 TA - P3 WU - PI	
6. AUTHOR(S) S. Kupiec and H.J. Caulfield					
7. PERFORMING ORGANIZATION NAME(S) AND ADDRESS(ES) Alabama A&M University Department of Physics P.O. Box 1268 Normal AL 35762				8. PERFORMING ORGANIZATION REPORT NUMBER N/A	
9. SPONSORING/MONITORING AGENCY NAME(S) AND ADDRESS(ES) Rome Laboratory (OCPB) 25 Electronic Pky Griffiss AFB NY 13441-4515				10. SPONSORING/MONITORING AGENCY REPORT NUMBER RL-TR-94-194	
11. SUPPLEMENTARY NOTES <u>Rome Laboratory Project Engineer: Rebecca Bussjager/OCPB/(315) 330-3261</u>					
12a. DISTRIBUTION/AVAILABILITY STATEMENT Approved for public release; distribution unlimited.				12b. DISTRIBUTION CODE	
13. ABSTRACT (Maximum 200 words) Within our previous report, we have described a digital computer architecture, the HOPLA, and algorithms that effectively exploit that architecture. Within the present report, we shall examine the theoretical performance of the HOPLA, implementing various configurations of the multiread function. The present report consists of the following. The first section consists of a review of the semi-quantitative analysis of the N^4 interconnect. In the next section, we apply this analysis to the case of the proposed HOPLA implementation. Proceeding with the results from this section, we then consider the required thresholds and reliability levels of the system under various operating conditions. Finally, we consider the effects of operation at very low power levels with an emphasis on the effects of shot noise.					
14. SUBJECT TERMS Holographic interconnect, Optical interconnect, Optical computing, High fan-in components				15. NUMBER OF PAGES 52	
				16. PRICE CODE	
17. SECURITY CLASSIFICATION OF REPORT UNCLASSIFIED	18. SECURITY CLASSIFICATION OF THIS PAGE UNCLASSIFIED	19. SECURITY CLASSIFICATION OF ABSTRACT UNCLASSIFIED	20. LIMITATION OF ABSTRACT SAR		

Table of Contents

Introduction.	1
1. Interconnect Analysis.	1
1.1. Layout and Overview.	2
1.2. Parameters for the Multiread Function.	3
2. Semi-Quantitative Constraints	4
3. Constraints Specific to the Multiread Function	7
3.1. Diffraction Effects.	7
3.1.1. The Morton Order	8
3.1.2. The Grey Coded Morton Order.	11
3.1.3 Hilbert Curve Order	13
3.2. Analysis of diffraction patterns	16
3.2.1. Effects upon Holographic Recording.	17
3.2.2. Diffraction Effects Upon Crosstalk	19
3.2.3. Analysis of Crosstalk Results	21
4. Power Consumption Considerations:	22
4.1. Power Consumption Under Conventional Conditions	22
4.2. Alternative Operation Scheme	24
4.3 Very Low Power Switching.	25
4.3.1. Threshold Values	26
4.3.2. Reliability Considerations	29
4.3.3. Implications of Low Power Operation.	31
4.3.4. The WPD Model	34
5. Conclusion	38
References	39

Accession for	
HTIS	CHUM
DHC	DD
Unlabeled	DD
JANUARY	
1980	
1981	
1982	
1983	
1984	
1985	
1986	
1987	
1988	
1989	
1990	
1991	
1992	
1993	
1994	
1995	
1996	
1997	
1998	
1999	
2000	
2001	
2002	
2003	
2004	
2005	
2006	
2007	
2008	
2009	
2010	
2011	
2012	
2013	
2014	
2015	
2016	
2017	
2018	
2019	
2020	
2021	
2022	
2023	
2024	
2025	
2026	
2027	
2028	
2029	
2030	
2031	
2032	
2033	
2034	
2035	
2036	
2037	
2038	
2039	
2040	
2041	
2042	
2043	
2044	
2045	
2046	
2047	
2048	
2049	
2050	
2051	
2052	
2053	
2054	
2055	
2056	
2057	
2058	
2059	
2060	
2061	
2062	
2063	
2064	
2065	
2066	
2067	
2068	
2069	
2070	
2071	
2072	
2073	
2074	
2075	
2076	
2077	
2078	
2079	
2080	
2081	
2082	
2083	
2084	
2085	
2086	
2087	
2088	
2089	
2090	
2091	
2092	
2093	
2094	
2095	
2096	
2097	
2098	
2099	
2100	
2101	
2102	
2103	
2104	
2105	
2106	
2107	
2108	
2109	
2110	
2111	
2112	
2113	
2114	
2115	
2116	
2117	
2118	
2119	
2120	
2121	
2122	
2123	
2124	
2125	
2126	
2127	
2128	
2129	
2130	
2131	
2132	
2133	
2134	
2135	
2136	
2137	
2138	
2139	
2140	
2141	
2142	
2143	
2144	
2145	
2146	
2147	
2148	
2149	
2150	
2151	
2152	
2153	
2154	
2155	
2156	
2157	
2158	
2159	
2160	
2161	
2162	
2163	
2164	
2165	
2166	
2167	
2168	
2169	
2170	
2171	
2172	
2173	
2174	
2175	
2176	
2177	
2178	
2179	
2180	
2181	
2182	
2183	
2184	
2185	
2186	
2187	
2188	
2189	
2190	
2191	
2192	
2193	
2194	
2195	
2196	
2197	
2198	
2199	
2200	
2201	
2202	
2203	
2204	
2205	
2206	
2207	
2208	
2209	
2210	
2211	
2212	
2213	
2214	
2215	
2216	
2217	
2218	
2219	
2220	
2221	
2222	
2223	
2224	
2225	
2226	
2227	
2228	
2229	
2230	
2231	
2232	
2233	
2234	
2235	
2236	
2237	
2238	
2239	
2240	
2241	
2242	
2243	
2244	
2245	
2246	
2247	
2248	
2249	
2250	
2251	
2252	
2253	
2254	
2255	
2256	
2257	
2258	
2259	
2260	
2261	
2262	
2263	
2264	
2265	
2266	
2267	
2268	
2269	
2270	
2271	
2272	
2273	
2274	
2275	
2276	
2277	
2278	
2279	
2280	
2281	
2282	
2283	
2284	
2285	
2286	
2287	
2288	
2289	
2290	
2291	
2292	
2293	
2294	
2295	
2296	
2297	
2298	
2299	
2300	
2301	
2302	
2303	
2304	
2305	
2306	
2307	
2308	
2309	
2310	
2311	
2312	
2313	
2314	
2315	
2316	
2317	
2318	
2319	
2320	
2321	
2322	
2323	
2324	
2325	
2326	
2327	
2328	
2329	
2330	
2331	
2332	
2333	
2334	
2335	
2336	
2337	
2338	
2339	
2340	
2341	
2342	
2343	
2344	
2345	
2346	
2347	
2348	
2349	
2350	
2351	
2352	
2353	
2354	
2355	
2356	
2357	
2358	
2359	
2360	
2361	
2362	
2363	
2364	
2365	
2366	
2367	
2368	
2369	
2370	
2371	
2372	
2373	
2374	
2375	
2376	
2377	
2378	
2379	
2380	
2381	
2382	
2383	
2384	
2385	
2386	
2387	
2388	
2389	
2390	
2391	
2392	
2393	
2394	
2395	
2396	
2397	
2398	
2399	
2400	
2401	
2402	
2403	
2404	
2405	
2406	
2407	
2408	
2409	
2410	
2411	
2412	
2413	
2414	
2415	
2416	
2417	
2418	
2419	
2420	
2421	
2422	
2423	
2424	
2425	
2426	
2427	
2428	
2429	
2430	
2431	
2432	
2433	
2434	
2435	
2436	
2437	
2438	
2439	
2440	
2441	
2442	
2443	
2444	
2445	
2446	
2447	
2448	
2449	
2450	
2451	
2452	
2453	
2454	
2455	
2456	
2457	
2458	
2459	
2460	
2461	
2462	
2463	
2464	
2465	
2466	
2467	
2468	
2469	
2470	
2471	
2472	
2473	
2474	
2475	
2476	
2477	
2478	
2479	
2480	
2481	
2482	
2483	
2484	
2485	
2486	
2487	
2488	
2489	
2490	
2491	
2492	
2493	
2494	
2495	
2496	
2497	
2498	
2499	
2500	
2501	
2502	
2503	
2504	
2505	
2506	
2507	
2508	
2509	
2510	
2511	
2512	
2513	
2514	
2515	
2516	
2517	
2518	
2519	
2520	
2521	
2522	
2523	
2524	
2525	
2526	
2527	
2528	
2529	
2530	
2531	
2532	
2533	
2534	
2535	
2536	
2537	
2538	
2539	
2540	
2541	
2542	
2543	
2544	
2545	
2546	
2547	
2548	
2549	
2550	
2551	
2552	

Introduction.

Within our previous report[1] we have described a digital computer architecture, the HOPLA, and algorithms which effectively exploit that architecture. Within the present report, we shall examine the theoretical performance of an HOPLA implementing various configurations of the multiread function.

The present report consists of five sections: The first section consists of a review of the semi-quantitative analysis of the N^4 interconnect. In the next section we shall apply this analysis to the case of the proposed HOPLA implementation. Proceeding with the results from this section, we shall then consider the required thresholds and reliability levels of the system under various operating conditions. Finally, we shall consider the effects of operation at very low power levels with an emphasis on the effects of shot noise.

1. Interconnect Analysis.

Within the present section we shall review the semi-quantitative constraints upon N^4 interconnects described in references [2] and [3]. We shall consider the impact of these constraints upon the general HOPLA designs, employing our current laboratory design as an example. We shall then consider the unique properties of our proposed multiread implementations with regard to the constraints cited.

1.1. Layout and Overview.

We shall now describe the idealized layout of an N^4 interconnect and define the variables employed.

The N^4 interconnect consists of three major components: A Page Oriented Holographic Memory (POHM) consisting of an array of adjacent Fourier transform holograms, a Spatial Light Modulator (SLM) sandwiched between a pair of lenses of focal length f and a detector array. The POHM and the detector array are located at one focal length to either side of the SLM as indicated within Figure 1.4. The arrangement of the detector array is proportional to that of the POHM array, with a detector located at the conjugate point of each hologram.

The operation of the hologram is as follows: A conjugate reconstruction beam illuminates the POHM array. Each of the holograms simultaneously project a different control mask upon the SLM and lens arrangement, and then focus upon the detector array. Since each control mask is projected at a differing angle, it comes to a focus at a different location on the detector array, specifically, the conjugate location of the hologram from which it originates. In this manner, each bright pixel within the control mask connects that location on the SLM to the detector associated with the mask. In this manner we may arbitrarily connect the contents of the SLM to the elements of the detector array.

Within our discussion of the properties of the N^4 interconnect, we shall employ the nomenclature of reference [4] unless otherwise noted. To wit: The SLM consists of an $N_s \times N_s$ arrangement of pixels, each pixel with a side dimension of p_s with a spacing of

d_s resulting in an overall dimension of S . The POHM consists of an $N_h \times N_h$ arrangement of holograms, each hologram having a diameter of p_h and a spacing of d_h resulting in an overall dimension of H . The detector array consists of an $N_d \times N_d$ arrangement of detectors, each detector with a side dimension of p_d with a spacing of d_d resulting in an overall dimension of H . The operating wavelength of the system is λ . Finally, the reconstruction beam angle is θ_r .

When employing Fourier transforms, we shall employ the nomenclature of reference [5] in preference to that of reference [3]. Specifically, when referring to Fourier transform pairs, we shall employ lowercase letters for the original function and uppercase letters for the associated Fourier transforms.

We shall define the function $ceil(x)$ as returning the smallest integer value which is greater than or equal to the value of the argument. For example $ceil(4.5)=5$ and $ceil(3)=3$. We shall denote the base 2 logarithm as \log_2

1.2. Parameters for the Multiread Function.

In the case of the multiread function, many of the parameters of the previous section are dependent upon the number of inputs to the function. Thus, given the parameters of the SLM it is possible to infer many of the remaining values.

As we have noted within our previous report[1], given 2^m inputs, the basic multiread function returns $2m$ outputs. Thus, given an SLM consisting of N_s^2 pixels, each pixel corresponding to an input, the corresponding value of m is:

$$m=2 \text{ ceil}[\log_2(N_s)] \quad [1]$$

Several additional outputs are required if we are to employ error correction within the multiread function. In the case of Extended Hamming Code (EHC), t error correction bits are sufficient to correct for $2^{t-1}-1$ address bits. As with address bits, the multiread function employs two outputs for each bit employed. Thus given a value of t such that:

$$m \leq 2^{t-1}-1 \quad [2]$$

We must incorporate $2t$ additional outputs in order to obtain error correction.

Once the number of outputs have been selected, it is then possible to determine the arrangement and dimensions of both the hologram and detector arrays. Given m inputs, the arrangement of the hologram array is:

$$N_h = \text{ceil}[\sqrt{(2m)}] \quad [3]$$

If we assume that the overall dimension H of the hologram is equal to that of the SLM S , then we may immediately infer the spacing of the holograms involved:

$$d_h = H/N_h \quad [4]$$

The arrangement of the detector array is, by necessity, always proportional to that of the hologram array (i.e. $N_d = N_h$). In most cases, the dimensions and arrangement of the detector are the same as those of the hologram array. This is convenient, in that it allows

the same resolution limits to be applied to both arrays. This is feasible, given that the total number of outputs employed within the multiread function is relatively small, and it is most likely that arrangements of discrete detectors would be employed. Which, in turn, allows for considerable flexibility in their arrangement. Within the current discussion we shall assume that the dimensions of the detector and hologram are equal (i.e. $d_d = d_h$).

2. Semi-Quantitative Constraints

We shall now review the general constraints upon the N^4 interconnect described within references [3] and [4].

We begin by defining several geometrical properties of the system. We designate the maximal angle of the beams incident upon the SLM as θ_{max} , which has the value of:

$$\theta_{max} = (1/2) \arctan\{H/(\sqrt{2}f)\} \quad [5]$$

We shall denote the maximal distance between the hologram plane and SLM plane as r which we approximate as $r \approx f \cos \theta_{max}$.

Given these geometrical factors we may then impose the first constraint. Assuming diffraction limited performance, it is necessary for each hologram within the array to be sufficiently large as to be able to resolve the individual pixels of the SLM. Reference [4] expresses this constraint as:

$$d_s \geq 2.44 \frac{\lambda H \sqrt{2}}{p_h \sin(2\theta_{max})} \quad [6]$$

Since the values of H , d_s and λ are generally fixed by practical considerations. The effect of this constraint is to set a lower limit upon the size of the individual holograms employed (p_h) as a function of the focal length f of the system. In general, we wish to select a value of f that allows for a value of p_h such that the individual holograms do not overlap (i.e.: $p_h \leq d_h$). This constraint is not absolute, in that the individual holograms may overlap, but such overlap results in reduced efficiency and increased levels of crosstalk. In addition, an array employing non-overlapping holograms may be used to implement the window set function, as per our previous report[1].

A second constraint upon the value of f is that as the value of f decreases, the value of θ_{max} increases. Broad variations of the incident angle result in several undesirable effects. Most notably, nearly every SLM that may be employed within the system displays a strong sensitivity to variations in angle. Reference [4] derives several limits upon the contrast level of polarization modulation based SLMs as a result of the variation in angle. These constraints are based upon the limits of the polarization components employed. The maximum contrast ratio R_m possible employing ideal polarization analyzers is:

$$R_m = \frac{4n^4}{\pi^2 \sin(\theta_{max})^4} \quad [7]$$

Where n is the index of refraction of the active material of the SLM. A similar degree of variation is encountered as a result of path length variations encountered within SLMs that employ linear birefringence[4]. Magneto optic devices differ from other devices in their angular sensitivity[4], but it is likely that path length variations alone will

lead to similar results. It is most likely that the angular sensitivity of the anti-reflection coating employed within magnetooptic SLMs [6] will predominate over simpler polarization effects. Obviously, given the high fan-ins associated with our architecture, it is very important to achieve the highest possible contrast within the system.

Besides the angular variation of the SLM, several other simpler geometric effects lead to angular sensitivity within the system. Most notably there is the elongation of the image beam projected upon the hologram or detector plane, which is proportional to $1/\cos\theta$, and the variation in intensity of the image, which is proportional to $\cos^4\theta$. Although these effects do complicate recording and playback, the bulk of the ill effects may be eliminated by proper calibration methods.

Table 1. summarizes the variables and equations that have been employed so far, and provides representative values for the prototype system that we have constructed.

3. Constraints Specific to the Multiread Function

Within the present section, we shall analyze the operation of an implementation of the multiread function upon an N^4 interconnect. We shall then discuss the constraints operating upon the system as a result of this analysis.

3.1. Diffraction Effects.

As we have previously noted, one of the primary advantages of the multiread function as a test pattern, is that it employs a regular and easily verified set of control masks. We shall now exploit this advantage to obtain explicit formulations of the Fourier

transform pairs of the control masks that we anticipate using. Given these transform pairs, we may then easily calculate the Fraunhofer diffraction pattern of a given mask, and employ it to analyze hologram formation and reconstruction.

3.1.1. The Morton Order

We shall first consider masks arranged employing the Morton order, as defined within Our previous report[1]. As we have noted previously, the control masks generated by the Morton order are identical to those employing the raster scan order with the exception of the assignment of the outputs. Figure 2.11 illustrates a set of Morton order control masks for a 256x256 input matrix.

As we may see, the required masks associated with the Morton order consist of a set of basic forms, and three 90° rotations of the each of these forms. We shall employ the index k to designate each basic form, in order of increasing resolution. For the sake of convenience we define three new variables, n, a and b :

$$n = \text{ceil}[\log_2(N_s)] \quad [8]$$

$$b_k = 2^{n-k-1} \quad [9]$$

$$a_k = 2^k \quad [10]$$

$$2a_k b_k = N_s \quad [11]$$

Using these variables we may define the basic forms of the Morton order mask. The k^{th} mask consists of a_k vertical bright stripes b_k pixels wide, interspersed with an equal number of dark stripes of equal width, the top stripe being dark. Figure 1 illustrates this arrangement. We further assume that the inter-pixel region is opaque.

Using the nomenclature and formulas of reference [5], we define the function *grate*:

$$\text{grate}(N, d, x) = \sum_{m=1}^{N/2} \{ \delta[x - (m + 1/2)d] + \delta[x + (m + 1/2)d] \} \quad [12]$$

The *grate* function consists of N delta functions, equally spaced with a separation of d . The Fourier transform of this function is well known [7]:

$$\text{GRATE}(N, d, x') = \frac{\sin(\pi N d x')}{\sin(\pi d x')} \quad [13]$$

Where x', y' are coordinates in the frequency plane

Given the *grate* function, it is possible to express the k^{th} Morton order mask $m_k(x, y)$ in terms of a series of separable convolutions:

$$m_k(x, y) = \text{grate}(N_s d_s y) \{ \text{grate}(a_k 2b_k d_s x) \\ * \text{grate}(b_k d_s x) * \delta(x - b_k d_s) \} * \text{rect}(x/p_s y/p_s) \quad [14]$$

Where $*$ denotes the convolution operator. The corresponding Fourier transform $M_k(x', y')$ is:

$$M_k(x', y') = \exp(-i\pi b_k d_s x') p_s^2 \text{sinc}(p_s x', p_s y') \\ \text{GRATE}(N_s d_s y') \text{GRATE}(a_k 2b_k d_s x') \text{GRATE}(b_k d_s x') \quad [15]$$

It is possible to rework the product of the rightmost two functions in order to obtain a more intuitive result:

$$\text{GRATE}(a_k 2b_k d_s x') \text{GRATE}(b_k d_s x') \\ = \frac{\sin(\pi 2a_k b_k d_s x')}{\sin(\pi 2b_k d_s x')} \frac{\sin(\pi b_k d_s x')}{\sin(\pi d_s x')} \quad [16]$$

given $2a_k b_k = N_s$

$$= \frac{\sin(\pi N_s d_s x')}{\sin(\pi d_s x')} \frac{\sin(\pi b_k d_s x')}{\sin(\pi 2b_k d_s x')} \quad [17]$$

Employing the double angle identity

$$= \frac{\sin(\pi N_s d_s x')}{\sin(\pi d_s x')} \frac{1}{2 \cos(\pi 2b_k d_s x')} \quad [18]$$

$$= \frac{\sin(\pi N_s d_s x')}{2 \sin(\pi d_s x')} \sec(\pi 2b_k d_s x') \quad [19]$$

Resulting in the following form of $M_k(x', y')$ is:

$$M_k(x', y') = (1/2) \exp(-i\pi b_k d_s x') p_s^2 \text{sinc}(p_s x', p_s y') \quad [20]$$

$$\text{GRATE}(N_s, d_s, y') \text{GRATE}(N_s, d_s, x') \sec(\pi 2b_k d_s x')$$

We may interpret this form of the Fourier transform as follows: With the exception of the first and last factors, the transform is identical to that of the blank SLM with all pixels set bright. The first term is simply a result of the shift theorem, indicating the asymmetric arrangement of the stripe pattern within the mask. The final term reflects the influence of the mask pattern upon the transformed image. Given that:

$$N_s/b_k = 2^{k+1} \quad [21]$$

We may see that the period of the secant function and the numerator of the *GRATE* function coincide, effectively suppressing any singularities encountered. The overall effect of the secant term is to emphasize the maxima that would occur if the stripe pattern were the sole component of the function. This pattern effectively “beats” with the pattern generated by the presence of pixels. It is important to note that, with the exception of those canceled by the secant function, the zeros of the *GRATE* function occur at the same period as the “all bright” SLM indicating a function consisting of a series of narrow, sharp peaks.

The generation of the masks required for a Morton order implementation of the multiread function requires two steps: First, the basic form masks $m_k(x,y)$ are generated for the values of $k=0,1,...(n-1)$. Then, each of these masks are subjected to three 90° rotations, resulting in the functions $m_k(-x,-y)$, $m_k(y,x)$ and $m_k(-y,-x)$. Obviously, the transforms of these masks may be generated in the same manner.

3.1.2. The Grey Coded Morton Order.

As we have seen within our previous report[1], if we employ the canonical Grey code enumeration, the pattern of the Morton order encoded masks changes. Although the m_0 mask and its rotations are still encountered, the remaining basic form masks incorporate a centered series of a_{k-1} bright vertical stripes of width b_{k-1} pixels. In order to obtain a full set of masks, the basic form masks are subjected to a single 90° rotation, and the light and dark pixels are interchanged in both the original form and the rotated form to obtain the required masks.

As in the last section, we may express the $k=1,2,...(n-1)$ masks as a series of convolutions:

$$m_{grey\ k}(x,y) = \text{grate}(N_s, d_s, y) [\text{grate}(a_{k-1}, 2b_{k-1}d_s, x) \quad [22] \\ * \text{grate}(b_{k-1}, d_s, x)] * \text{rect}(x/p_s, y/p_s)$$

We may note that this function is identical to that of the conventionally coded form, except for the absence of the $\delta(x-b_kd_s)$ term employed to offset the stripes in the original formulation. For this reason the Fourier transform is nearly identical to that of the previous function:

$$M_{grey\ k}(x', y') = (1/2)p_s^2 \text{sinc}(p_s x', p_s y') \quad [23]$$

$$GRATE(N_s d_s y') GRATE(N_s d_s x') \sec(\pi 2 b_{k-1} d_s x')$$

The results are identical, except for the presence of the $\exp(-i\pi b_{k-1} d_s x')$ phase factor, and the $k-1$ indices which indicate that the spatial frequency of the stripes in each mask is half that of the masks of the previous section. Otherwise, the analysis of the previous section is valid for this section.

As we have noted above, it necessary to interchange the bright and dark pixels within the images employed in order to obtain the required masks. For this reason it is necessary to calculate the Fourier transform of these inverted masks. We may achieve this result by subtracting the $m_{grey\ k}$ masks from an "all bright" SLM pattern to obtain the inverted $m'_{grey\ k}$ mask. The corresponding transform is:

$$M'_{grey\ k}(x', y') = (1/2)p_s^2 \text{sinc}(p_s x', p_s y') \quad [24]$$

$$GRATE(N_s d_s y') GRATE(N_s d_s x') [2 - \sec(\pi 2 b_{k-1} d_s x')]$$

We may see that the added terms associated with this function result from the presence of half width bright stripes appearing at the edge of the masks.

In order to generate all of the masks required for the Grey coded Morton order, it is necessary to generate the $m_{grey\ k}(x, y)$ and $m'_{grey\ k}(x, y)$ masks for the values $k=1, 2, \dots, (n-1)$. It is then necessary to rotate these masks 90° to obtain the $m_{grey\ k}(y, x)$ and $m'_{grey\ k}(y, x)$ masks. It is also necessary to generate the $m_0(x, y)$, $m_0(-x, -y)$, $m_0(y, x)$ and $m_0(-y, -x)$ masks. Once again, the transforms of these masks may be generated in the same manner.

3.1.3 Hilbert Curve Order

Another of the orders that we may employ to generate control masks is the Hilbert curve order. As we have noted previously, the masks generated either produce checkerboard pattern masks, or masks arranged in a fractal pattern. We have argued that the intricate texture of fractal patterns should result in more uniform diffraction patterns. Unfortunately, it is the same intricate texture that greatly complicate the evaluation of the Fourier transform. Although simple expressions for such transforms are not presented, we do present a recursive expression that should greatly simplify automatic evaluation of the transforms.

We shall begin by considering the Fourier transform of the checkerboard control masks. We may express a checkerboard as the superposition of two grids, each offset from the origin by one quarter the spacing of the grid:

$$ch(N,d,x,y)=grate(N/2,2d,x,y) \quad [25]$$

$$*[\delta(x-d/2,y-d/2)+\delta(x-d/2,y+d/2)]$$

where

$$grate(N,d,x,y)=grate(N,d,x)grate(N,d,y) \quad [26]$$

The Fourier transform is simply:

$$CH(N,d,x',y')=2GRATE(N/2,2d,x',y')\cos[\pi d(x'+y')] \quad [27]$$

In the k^{th} mask, each square is $b_k \times b_k$ pixels large. Incorporating the effects of pixels:

$$m_{check\ k}(x,y)=grate(b,d_s,x,y)*ch(2a,bd_s) \quad [28]$$

$$*rect(x/p_s,y/p_s)$$

Resulting in the Fourier transform:

$$M_{check\ k}(x,y)=GRATE(b,d_s,x,y)GRATE(a,2bd_s,x,y) \quad [29]$$

$$\cos[\pi d_s(x' + y')]p_s^2 \text{sinc}(p_s x', p_s y')$$

Reworking the *GRATE* functions in the same manner as the last section:

$$M_{check\ k}(x',y')=GRATE(N_s,d_s,x',y')\cos[\pi d_s(x' + y')] \quad [30]$$

$$\text{sec}(\pi b d_s x')\text{sec}(\pi b d_s y')p_s^2 \text{sinc}(p_s x', p_s y')/2$$

This transform is similar to those in the previous section with the exception of the diagonal cosine term, which arises from the initial offset of the two grids.

In order to generate the required masks, it is also necessary to generate a 90° rotation of the $m_{check\ k}$ mask.

We shall now consider the evaluation of the Fourier transforms of the fractal control masks. In our previous report[1] the primary means of generating the Hilbert curve was to employ Butz's algorithm[8], which was well suited to simple generation by computers. We shall now describe a more intuitive means of generating the Hilbert curve and derive an appropriate recursive formulation of our masks.

We shall now consider the "seed" method of generating a Hilbert curve[9]. We begin with the simplest possible approximation to the Hilbert curve, one which connects four points, and employ it as our seed value, as per figure 1. We then generate four half size copies of the seed curve and arrange them in the manner illustrated in figure 1 connecting adjacent end points. This results in the next finer Hilbert curve. If we repeat the process this time, employing our previous result as the seed value, then we obtain the next finer Hilbert curve. By recursively applying this method, we may generate any resolution of Hilbert curve required.

We may employ the same method to generate our control masks. If we use the two lowest resolution masks (those associated with the two most significant bits) as our seed masks, we may recursively generate the remaining finer masks in the same fashion as we generated the Hilbert curve (as per figure 1). The reason why this works is that a control mask of a given resolution is only dependent upon the Hilbert curve of the same resolution.

We may describe this in terms of a recursive formula, if $m_k(x,y)$ is the function for the k^{th} mask with dimensions $S \times S$, then the formula for $m_{k+2}(x,y)$ is:

$$\begin{aligned} m_{k+2}(x,y) = & m_k(2\{y+S/4\}, 2\{x+S/4\}) \\ & + m_k(2\{x+S/4\}, 2\{y-S/4\}) \\ & + m_k(2\{x-S/4\}, 2\{y-S/4\}) \\ & + m_k(2\{-y-S/4\}, 2\{-x-S/4\}) \end{aligned} \quad [31]$$

The Fourier transform of this formula is:

$$\begin{aligned} M_{k+2}(x',y') = & (1/4) \exp[i\pi(x'+y')S/2] M_k(y'/2, x'/2) \\ & + (1/4) \exp[i\pi(x'-y')S/2] M_k(x'/2, y'/2) \\ & + (1/4) \exp[-i\pi(x'+y')S/2] M_k(x'/2, y'/2) \\ & + (1/4) \exp[i\pi(-x'+y')S/2] M_k(y'/2, x'/2) \end{aligned} \quad [32]$$

Thus given the value of $M_0(x',y')$ and $M_1(x',y')$ it is possible to compute the Fourier transform of any desired fractal control mask. The task may be further simplified by defining $m_0(x,y)$ and $m_1(x,y)$ in terms of delta functions. For example, the values for normal enumeration are:

$$m_0 = \delta(x-S/4, y-S/4) + \delta(x-S/4, y+S/4) \quad [33]$$

$$m_1 = \delta(x+S/4, y-S/4) + \delta(x-S/4, y+S/4) \quad [34]$$

The values for the Grey code enumeration are:

$$m_0 = \delta(x-S/4, y-S/4) + \delta(x-S/4, y+S/4) \quad [35]$$

$$m_1 = \delta(x-S/4, y-S/4) + \delta(x+S/4, y-S/4) \quad [36]$$

Figure 2 illustrates the form of these seed values. The resulting mask patterns may then be "filled out" by convolution.

Given the structure of the recursive definition, it is possible to anticipate a smoother set of transforms than the Morton order. On the other hand, it is also clear that the high degree of self-similarity within such a fractal process will ensure a considerable number of local maxima.

3.2. Analysis of diffraction patterns

Having determined Fourier transforms of the various control masks that may be encountered within our project, we may then calculate the impact of these functions upon our capacity to record and reconstruct our desired control masks.

We shall now consider the following arrangement, our desired mask $m_k(x, y)$ is illuminated by a beam of collimated coherent light, and then propagates a distance l before encountering a lens of focal length f and then continues to the back focal plane of the lens as per figure 3. The resulting Fraunhofer diffraction pattern is given by the following formula[5] (discarding constant phase factors):

$$I(x, y) = (A_0 / i\lambda f) \exp\{i(2\pi/\lambda)(l+f)\} \exp\{i\pi(f-l)/(\lambda f^2)(x^2+y^2)\} M_k(x/\lambda f, y/\lambda f) \quad [37]$$

Where A_0 denotes the net intensity of the diffracted image. Employing this equation we may determine the diffraction pattern impinging upon the hologram plane during recording and upon the detector plane during reconstruction.

3.2.1. Effects upon Holographic Recording.

Given the ideal diffraction pattern generated by a given control mask, we may make several observations upon the influence of the pattern upon the recording and reconstruction of the holographic image.

We shall first consider the holographic recording process. In the case of a thin hologram, the image beam $I(x,y)$, consisting of the diffraction pattern of our desired mask is combined with an plane wave which serves as the reference beam $R(x,y)$:

$$R(x,y) = A_0 \exp[i(2\pi/\lambda) \sin \theta_0 x] \quad [38]$$

The two beams combine and interfere at the surface of the holographic plate to form an intensity pattern which is recorded by the photographic material. The recorded intensity pattern may be expressed as:

$$U(x,y) = [R(x,y) + I(x,y)]^2 \quad [39]$$

$$U(x,y) = [R(x,y) + I(x,y)][R(x,y) + I(x,y)]^* \quad [40]$$

$$U(x,y) = R(x,y)R(x,y)^* + I(x,y)R(x,y)^* + R(x,y)I(x,y)^* + I(x,y)I(x,y)^* \quad [41]$$

Where $*$ denotes the complex conjugate operation. Each term of this well known equation designates a feature of the resulting hologram. The first term RR^* is merely the constant bias introduced by the presence of the reference beam, while the fourth term II^* is the autocorrelation function of the control mask being recorded forming the intermodulation term. The second and third terms are the components that contribute to

the reconstruction of the image and its complex conjugate.

We may determine several effects arising from the recording process. Obviously, we do not wish to generate a pattern with features smaller than that of resolution of the film employed v . Given that the finest features of the diffraction patterns of the Morton order masks and the Checkerboard masks are the zeros of the $GRATE[N_s, d_s, x/(\lambda f), y/(\lambda f)]$ function. Given the minimal spacing of these values, the resulting constraint takes the form:

$$v \leq \lambda / N_s d_s \quad [42]$$

Which is identical to the constraint arrived at by reference [3]. In addition, the resolution of the interference pattern generated between the image and reference beam should be within that of the film. If we assume, for simplicity, the Morton order and that $l=f$ (allowing us to discard the quadratic phase factor of equation[5]) then we may assume that $I(x,y)$ is of piecewise continuous phase. The local interference pattern is proportional to:

$$\sin((2\pi/\lambda)\sin\theta_r x) \quad [43]$$

Resulting in the constraint:

$$v \leq \sin(\theta_r)/\lambda \quad [44]$$

The other effect arising during the recording process which is of interest, is the influence of the $I I^*$ intermodulation term. The overall effect of this term is to introduce noise into the reconstruction process, both directly, and by exhausting the dynamic range of the recording material. For this reason, when recording a transmission hologram it is desirable to select a ratio between the image beam intensity and the reference beam intensity which is sufficient to allow the other terms to predominate over the effects of

this intermodulation. Unfortunately, in the case of images which possess sharply peaked autocorrelation functions, it is impossible to select a ratio which is valid for all areas of the diffraction pattern. The practical result of this effect is a loss of overall diffraction efficiency and contrast. Within our previous report[1] we have considered various means by which we may counteract this effect. Of course, the simplest method to avoid such effects is to employ masks that contain relatively smooth autocorrelation patterns. As we have noted previously, this is one of the primary advantages of the Hilbert order control masks.

Our holographic recording process differs considerably from that of the simple thin hologram model. The holographic media employed is sufficiently thick as to display properties of both thin and thick holograms. In addition our processing employs rehalogenation bleaching, resulting in phase holograms. In fact, the specific process of grain migration employed serves as a high-pass spatial filter, eliminating constant and low frequency terms from the recording process. In addition, the high degree of aberration of the lenses employed, as well as the variations in propagation distance for different channels result in considerable variation from the ideal diffraction patterns described. For this reason, the validity of theoretical models, beyond setting fundamental constraints upon operation, may prove to be rather questionable.

3.2.2. Diffraction Effects Upon Crosstalk

We shall now consider the effect of diffraction upon crosstalk between separate channels, both within the input and output functions. We shall then discuss the influence of various features of our specific application upon the effects of crosstalk.

We begin by considering the reconstruction of our control masks. We begin by assuming that we have selected a reference beam angle sufficient such that the reconstruction beam clears the remainder of the components after illuminating the hologram. In addition we shall assume that our processing is sufficiently linear as to largely suppress the presence of higher diffraction orders, and generates an image of high fidelity. Given these assumptions, the primary source of distortion in reconstruction is the finite size of the hologram. We may represent this effect by convolving the original hologram by the Fourier transform of the aperture, i.e.:

$$m_{recon}(x,y)=m(x,y)*(\pi d_h/4)somb[r/(d_h\lambda f)] \quad [45]$$

The net effect of which is to introduce a spreading of the boundaries of the control mask. This, combined with the finite contrast of both the holographic image and the SLM cause true input values within the false regions of the control mask to have non-zero values. A sufficient number of these values shall result in the generation of false alarms. For this reason it is necessary to examine the tradeoffs between resolution and contrast when selecting the focal length of the system. It is important to note that in the case of Morton order masks, it is possible to blur the mask along the direction of the stripes with no ill effects. Thus it may prove possible to obtain lower crosstalk by tessalating the hologram array with oblong masks.

The second source of crosstalk within the system arises from the diffraction pattern generated at the detector location. The signal traveling from the SLM to the detector encounters the same diffraction effects as the image beam encounters during exposures. Therefore, the outer lobes of the diffraction pattern will overlap with adjacent detectors causing crosstalk. In the worst case, the input stored upon the SLM contains a

random distribution of pixels, resulting in a diffraction pattern corresponding to that of a single pixel. Assuming operation near the diffraction limit, a worst case 4% degree of crosstalk has been numerically calculated within reference [2]. It is therefore once again desirable to select a value of f such that the system is well within diffraction limits.

3.2.3. Analysis of Crosstalk Results

At this point, it is important to make several important observations with regard to the specific effects of crosstalk upon the multiread function. Given m outputs, at most $m/2$ outputs may be dark at any time. If s outputs are dark, then the maximum number of true values within the inputs that may be true is $2^{m/2-s}$. In such a worst case situation, s light outputs complementary to that of the dark values are connected to half of the true values ($2^{m/2-s-1}$), and the remaining outputs are connected to a quarter of the true values ($2^{m/2-s-2}$). Similarly, it is possible to show, using hash collision formulas, that small numbers (~ 8) of randomly activated pixels have a high probability of activating all outputs.

In addition, given that the error correction methods described within our previous report are particularly sensitive to false negatives, allowing us to set our threshold of detection at a relatively high level while retaining high reliability.

The practical implications of these observations are that if we segregate complementary outputs, we may calculate our maximum level of tolerable crosstalk assuming that only a quarter of the input values are activated. Thus if c_0 is the maximum crosstalk arriving at any one output channel, and p_0 is the intensity of a single true pixel, then the maximum tolerable size of the SLM is:

$$N_s \leq \sqrt{(2/c_0)}$$

[46]

In reality, the maximum level of tolerable crosstalk is certainly much higher, since the distribution of the true values in the worst case, are in the same form as an one of the control mask, resulting in much tighter diffraction pattern, than previously noted. In the case of applications such as single pixel detection, or the detection of smaller window sets, the crosstalk limitation should be considerably smaller.

Finally, the form of the algorithms employed may be made resilient to crosstalk induced errors. For example, in the case of the second algorithm, the only effect of false dark values is to cause a greater number of cycles to be used in the execution of the algorithm.

4. Power Consumption Considerations:

We shall now consider the power required to operate our proposed system under various modes of operation.

4.1. Power Consumption Under Conventional Conditions

We shall begin by considering the simplest mode of operation for our proposed system, what we shall refer to as conventional operation. Under conventional operation, the holographic array is uniformly illuminated by a flash of light sufficiently intense as to trigger any detector that should record a bright result.

Under such a situation, it is necessary to provide each pixel of each control mask twice the sufficient energy to activate the detector element which it is connected to. If we set P_0 to twice the value of the threshold, and assume $2m$ outputs then the total conventional power consumption P_T is equal to:

$$P_T = (P_0 N_s^2 m) / (e_h \alpha q_{eff}) \quad [47]$$

Where e_h is the diffraction efficiency of the hologram employed, α is the net losses due to the attenuation of the SLM and the effects of diffraction and q_{eff} is the quantum efficiency of the detector. These figures are particularly high, since the multiread function employs masks that illuminate half of the SLM at any one time.

It is possible to double the number of operations involved without increasing the energy cost by implementing both the l and the d functions in the same architecture. The polarization encoding scheme described within our previous report[1] is a specific example. The power advantage encountered in this case is a result of the fact that the light discarded within the evaluation of the l function is employed within the evaluation of the d function.

Given that the total number of effective logical operations performed in the evaluation of the multiread function is $2mN_s^2$ the energy required per operation is $P_0 / (e_h \alpha q_{eff})$ a value comparable to that of conventional systems, a result of worst case operations occurring when a single pixel is activated. Of course, the HOPLA performs the entire set of operations simultaneously with a far smaller number of independent active elements.

4.2. Alternative Operation Scheme

In the previous section, we assumed that it was necessary to provide each pixel within the input with sufficient energy to independently trigger the threshold of each of the detectors to which it was connected. When, as in most cases, multiple pixels are active the additional energy is effectively wasted. In the case of the HOPLA, the power which is distributed to each pixel is dependent upon the level of illumination of the hologram associated with a given detector. This provides a means, in theory, of limiting the amount of energy required for the evaluation of each output.

Our proposed scheme for limiting the net quantity of power expended upon evaluation is as follows: Each (non-overlapping) hologram within the system is independently illuminated by a laser of constant power output. The detector array employs integrating detectors, which generate an output signal as the threshold of the unit is reached. Once the output signal is generated, the corresponding illumination laser is deactivated. The result of this scheme that each true value received is only sufficient to trigger the threshold, and the total power expended is the threshold power times the portion of the control mask obscured. The power expended in the evaluation of a false signal remains the same as that of the conventional operation. The average power consumption of the resulting architecture will be greatly reduced.

Obviously, such a scheme of operation is not a very practical mode of operation, but, such a configuration does allow for the evaluation of the one of the more intriguing possibilities associated with this architecture, switching which is achieved at exceedingly low optical power.

4.3 Very Low Power Switching

We have seen that within the alternative operating scheme the average amount of energy reaching each active element is equal to twice the threshold value of the active element. Under ideal conditions this value is limited by the effects of shot noise. Under such circumstances, the required threshold energy may be exceedingly low. Given that each active component preforms the equivalent of a large number of individual logical operations the potential cost per each operation is potentially smaller than any other known scheme for evaluating logical operations. Within the present section, we shall first consider the possible energy costs involved and then argue the significance of this figure.

When the alternative operating scheme is in use, the energy δ_e employed to switch each detector or active element to achieve an output is equal to the difference between the threshold value and the background level detected when a false value occurs. We shall now consider the minimum practical value for this threshold.

Let us consider the wavefront from one of the holograms immediately after it has passed through the SLM. The pattern consists of a plane wave containing the product of the input signal and the control mask. The only information contained within this wavefront is the locations of the inputs which are transmissive, and the direction of propagation. Between this point and the detector the wavefront converges to generate the signal which results in the output. Between these two points the computation occurs. The total energy contained within the wavefront mediating the operation is equal to the switching energy. As we have seen, it may require considerably more energy to set up the computation, but this additional energy does not take part in the actual computation. For this reason we may contend that the actual power employed to actually mediate the

computation is equal to the switching power.

It is therefore desirable to determine the smallest threshold value that may be employed to operate the system. Given that we are employing the alternative operating scheme, the influence of crosstalk is negligible, since each detector shall only receive sufficient energy to trigger it. If we employ a stable, single mode laser, the only absolute limit to the point at which we may set out threshold is the presence of Poisson shot noise[10]. This noise occurs as a result of the quantization of light, and serves as a source of noise that cannot be eliminated from the present arrangement.

4.3.1. Threshold Values

We shall thus calculate the required threshold under the shot noise limit. At the level at which shot noise becomes appreciable, the effects of the quantization of light are present and we must treat the intensity pattern impinging upon the detector as a collection of photons. We shall employ the semi-classical model for photoelectric detection[11], assuming that the mean number of photon counts that may be anticipated at a given sampling area over a given amount of time is proportional to the classical irradiance anticipated at that same point:

$$K_{mean} = I^2 \lambda / h \quad [48]$$

Where I^2 is the classical intensity over the sample area and K_{mean} is the average number of photon counts encountered. In the case of stable single mode laser radiation, the distribution of the number of photon counts about the mean is a function of

the Poisson distribution[11]:

$$P(K, K_{mean}) = (K_{mean}^K / K!) \exp(-K_{mean}) \quad [49]$$

Where $P(K, K_{mean})$ is the probability of K counts occurring during a given sampling period. Note that K is always an integer value, and P is a discrete probability function.

Given the presence of such noise, we wish to devise an optimal means of discerning the presence of a signal within the noise, and then determining the degree of error arising from such noise.

We begin by defining the nature of the signal that we wish to detect. During each sampling period, our signal may be in either of two states, true (bright), or false (dark). In the false or dark state, an average of n_b counts are received, due to the presence of a constant background bias. In the case of a true or bright state, an average of $(n_s + n_b)$ counts are received, consisting of the background signal and a signal from at least one true input. Of course, the signals arising from either state are subject to variations arising from shot noise. For this reason, it is necessary to devise a strategy for deciding whether a given sample value arises from a bright or dark state.

We shall employ the Maximum Likelihood (ML) decision strategy. This strategy selects the state that is most probable given the sample value. Given a sample of K counts, we shall assume that it is a result of a bright state when the probability of it occurring is greater than that of dark state:

$$p(K, (n_s + n_b)) > p(K, n_b) \quad [50]$$

Given that the two probability functions only intersect at a single point, it is possible to represent this decision as a threshold:

$$K > K_T \quad [51]$$

Where K_T is defined by the expression:

$$p(K_T, (n_s + n_b)) = p(K_T, n_b) \quad [52]$$

Which we may express as:

$$[(n_s + n_b)/K_T!] \exp(-n_s - n_b) = [n_b/K_T!] \exp(-n_b) \quad [53]$$

Taking the natural logarithm (\ln) of both sides we obtain:

$$\begin{aligned} K_T \ln(n_s + n_b) - \ln(K_T!) - (n_s + n_b) = \\ K_T \ln(n_b) - \ln(K_T!) - n_b \end{aligned} \quad [54]$$

Cancelling common terms, we obtain:

$$K_T = n_s / \ln[1 + (n_s/n_b)] \quad [55]$$

Thus we have obtained the expression for an optimal threshold given our initial criteria.

4.3.2. Reliability Considerations

Given that the probability distributions associated with the two states we wish to measure overlap to some extent, some error arising from statistical fluctuation will occur. In the case of a threshold system we may express the probability of error P_e in the form of the following equation (assuming that K_T has been rounded off to the nearest integer value):

$$P_e = \sum_{K=0}^{K_T} p(K, (n_s + n_b)) - p(K_T, (n_s + n_b))/2 + \sum_{K=K_T}^{\infty} p(K, n_b) - p(K_T, n_b)/2 \quad [56]$$

Where the first and second terms correspond to the cumulative probability of a bright sample having a value less than the threshold value (resulting in a false dark result), and the third and fourth terms correspond to the cumulative probability of a dark sample having a value greater than that of the threshold value (resulting in a false bright result).

Unfortunately, although the above equation results in a precise value for the anticipated error rate, it is very difficult to accurately evaluate for large values of K (i.e. $K \gg 10$) due to the presence of factorial values within the expression for the Poisson distribution. Under such circumstances, it is possible to approximate the Poisson distribution in the form of a normal distribution with a mean value of K_{mean} and a standard distribution of $\sqrt{K_{mean}}$. Under such circumstances it is possible to approximate the value of P_e by the use of the error function $erf(x)$:

$$P_e \approx 1 + (1/2)erf\{[K_T - (n_s + n_b)]/\sqrt{2(n_s + n_b)}\}/2 - (1/2)erf\{(K_T - n_b)/\sqrt{2n_b}\} \quad [57]$$

Employing this approximation we may calculate the probable rate of error for large values of n_s and n_b .

In the case of our present architecture, we may express the value of n_b in terms of n_s and the contrast ratio R :

$$n_b = (n_s N_s^2) / 4R \quad [58]$$

We may then calculate the value of P_e as a function of the value of R and n_s :

n_s	R			
	10	100	1000	2000
100	0.9304	0.7825	0.3860	0.2236
200	0.9017	0.6963	0.2202	0.0852
300	0.8798	0.6326	0.1332	0.0350
400	0.8613	0.5809	0.0830	0.0149
500	0.8452	0.5371	0.0526	0.0065
600	0.8306	0.4990	0.0337	0.0029
700	0.8173	0.4652	0.0218	0.0013
800	0.8049	0.4350	0.0142	0.0006
900	0.7933	0.4077	0.0093	0.0003
1000	0.7824	0.3828	0.0061	0.0001

Table 2 Probability of error P_e as a function of n_s and R in the case $N_s=256$.

Examining this table we may immediately deduce several facts. The first is that a high contrast ($\sim >1000$) SLM is required in order to achieve reliable low power operations. Secondly, given high contrast operation, reliable operation may be achieved with values of n_s as low as 900-1000, assuming the absence of other sources of noise.

The selection of a specific value for n_s is dependent upon the raw value of probable error that may be tolerated within the system. This quantity, in turn, is based

upon the degree of error correction that the system is capable of and the number of output errors that may be tolerated within the system. As we have shown within our previous report[1] the applications that we have proposed for the HOPLA incorporate a high degree of redundancy which confers a high level of resistance to error. For this reason, it is conceivable that reliable operation may be achieved with values of n_s as small as 900 (assuming $R=1000$). If higher levels of reliability are required, operation at $n_s=1000$ should be sufficient.

4.3.3. Implications of Low Power Operation.

Although the results of the previous two sections are quite straightforward, the implications of these results are quite significant. The reason for this is that each of our operations corresponds to $N_s/2$ logical operations. In the case of $N_s=256$ this corresponds to 32,768 effective dyadic logical operations being mediated by ~1000 photons. Paradoxically, each photon would appear to be mediating multiple logical operations. Within this section, we shall account for this apparent paradox and discuss its implications.

We may gain insight into this problem by noting that none of the photons mediating a given operation interact. This implies that each photon performs the entire operation independently. Under such an interpretation, the need for multiple photons arises from the need for a sufficient statistical sample to overcome the random nature of the individual outcomes. Under such an interpretation, our computer corresponds to a variation upon the well known problem of individual photons propagating through a double-slit aperture[12]. In both cases the location of each photon at the aperture (SLM)

is indeterminate, and its trajectory is dependent upon the configuration of the entire aperture.

It is important to note that although each operation corresponds to the equivalent of thousands of dyadic logical operations its result is always a single bit of information. For this reason, we may interpret our operations as the measurement of specific parameter of the aperture (input SLM) which must always take one out of two possible states. Under such an interpretation, the number of photons required to measure a single bit of information is quite reasonable when compared with comparable operations performed within optical communications[10].

The desirability of mediating a large number of dyadic logical operations by means of a small number of photons is that the effective energy cost per individual logical operation is exceedingly low. The effective amount of energy consumed per effective logical operation E_{op} may be expressed as:

$$E_{op} = (2n_s hc) / (N_s^2 \lambda) \quad [59]$$

Where h is Planck's constant and c is the speed of light. In the case of $n_s=1000$, $\lambda=514 \text{ nm}$ and $N_s=256$ the value of E_{op} is equal to 1.179×10^{-20} Joules. In comparison, the energy of an individual photon at $\lambda=514 \text{ nm}$ is equal to 3.865×10^{-19} Joules.

It has been postulated[13-15] that the minimal amount of energy that must be consumed to perform a single dyadic logical operation is equal to $\ln(2)k_B T$ where k_B is Boltzmann's constant and T is the temperature (Kelvin) of the switching mechanism. For a value of $T=0^\circ \text{K}$ the value of $\ln(2)k_B T = 2.614 \times 10^{-21}$ Joules. The basic rationale for such a

limit is that devices operating under such a limit would switch randomly as a result of background thermal fluctuations. An alternative interpretation of the of this limit is that conventional logical operations discard input information and consequently increase the entropy of the system in doing so. The impact of such a limit is that the waste heat generated by such energy consumption limits the ultimate size and speed of the logic gates involved.

A broad variety of schemes have been proposed for logic gates that are capable of operating at power consumption levels below that of the limit cited[16]. Many of these schemes employ the concept of Conservative or Reversible logic, a system of logic which retains sufficient information at each stage of computation to allow for the reversal of the entire computation. Since the process is reversible, the entropy associated with the data being processed remains constant, providing for the possibility of implementing such logic with arbitrarily low power consumption. Although a great many schemes for low power implementation of conservative logic have been proposed[16], to date no practical physical implementation exists.

If we compare the effective energy consumption of our operations against that of the optimal limit we find that $E_{op}/[ln(2)k_B T]=4.512$ indicating that our effective energy cost is quite nearly that of the proposed limit. It is equally obvious that if we were able to achieve reliable operation at $n_s=220$ (assuming increased SLM contrast) the value of E_{op} would actually be less than that of $ln(2)k_B T$ implying a violation of the proposed limit. Furthermore, it is obvious that there is no good reason to believe that the effects of the proposed limit will come into effect at this signal level, especially given that the signal actually received by the switching element is several thousand times more intense than the proposed energy limit. For this reason, it would appear that low power operation of

our proposed architecture allows for computation at an energy cost below that of previously considered limits.

4.3.4. The WPD Model

The concept that optics could be used to simultaneously evaluate a large number of logical operations at a exceedingly low energy cost was originally proposed by Caulfield and Shamir[2]. They postulated that within certain optical computer architectures, the energy required to evaluate a given problem did not depend upon the complexity of the operation but rather the complexity of the output. In order for an architecture to act in this fashion it must have two properties. It must be "complete", that is, when performing a given operation each photon must have the same range of possible trajectories. Secondly the system must be "coherent", that is the photons employed must have sufficiently similar properties as to propagate through the system in an identical manner. In other words, the individual photon trajectories must be ergodic for each operation. Caulfield has dubbed such a strategy Wave Particle Duality (WPD) computing, although the term single-photon computing would be equally descriptive. Two examples of optical architectures which are capable of WPD operations are optical correlators[2] and our present architecture.

A variety of arguments have been advanced citing various possible flaws within the WPD model. We shall now address such arguments.

A variety of arguments rest upon the misconception that the WPD model consists of a means of implementing some form of conservative logic and is consequently subject to weaknesses associated with that model. Although the WPD model bears certain

abstruse similarities to conservative logic models, it is radically different in most respects. Each operation within the WPD model employs a large number of inputs and discards the bulk of this information to obtain a single bit output. In comparison conservative logic operations are dyadic and retain all of the information associated with the input, allowing for the reversal of the operation if necessary. Within the WPD model, each switching element consumes considerably more energy than that present within the thermal background, assuring a reliable and irreversible state transition. Within conservative logic, each logic gate consumes a negligible amount of energy and may be subject to reversal during computation. Finally, the WPD model accepts a fixed energy cost for each output which it seeks to amortize by the complexity of the operations performed. In comparison, conservative logic systems presume that operations may occur at no energy cost, and that a small amount of energy is consumed to ensure forward operation.

Given the differences between the WPD model and the conservative logic model which we have cited above, it is obvious that it is immune to several of the major problems associated with the latter model. The WPD model is not subject to "arrow of time" problems in that it employs irreversible switching at each stage of computation, allowing for fixed bounds on the speed and reliability of computation. Since it need not be reversible, a WPD computer does not require retaining a large number of garbage bits as conservative logic systems require. Finally since each switching device operates at energy levels considerably in excess of the thermal limit they may be implemented without recourse to exotic physical processes, such as required for proposed implementations of conservative logic.

Another possible fallacy associated with our reasoning is that the proposed limit holds only for dyadic logic operations and that the use of high fan-in operations amounts to an evasion of the limit. It is most certainly true that the WPD method achieves its low effective power consumption by means of high fan-in operations. But, if such a method allows us to implement logical functions with comparable reliability, yet at intrinsically lower power dissipation levels, there is no good reason why such a method is not valid. In the history of logic design, a variety of different means of implementing digital logic have been employed, the rationale for all such methods has always been superior performance.

A similar objection to WPD methods is that they are intrinsically analog. In reality, all known means of implementing digital logic are "analog" in nature. The criteria for a digital logic device is that it accept discrete inputs and generate discrete, deterministic outputs. Obviously, it is more difficult to implement high fan-in digital logic, but the logic remains digital.

It may be argued that high fan-in operations are uncommon and therefore not well suited to the implementation of general purpose logic. Our previous report illustrated that it is possible to implement arbitrary finite automata by the use of high fan-in digital logic, as well as ample evidence for a variety of useful algorithms which optimally exploit high fan-in operations. Although it is not possible to solely employ high fan-in logic, it is possible to ensure that such operations predominate within most practical operations.

It has been argued that it is possible to indefinitely inflate the effective number of logical operations ascribed to our scheme. Such an argument claims that operations

which do not contribute to our results or that the information content of the input has been over estimated. Examination of the interconnection patterns described within our previous report reveals the following facts: Each bit within the input is independent of the state of any other and both of its possible states are equally probable, assuring maximal information content. Each input bit triggers a set of outputs which are unique to that bit and necessary to proper operation of the algorithm. Finally, any attempt to subdivide input bits (so as to inflate the number of operations) would not only fail to generate additional information but also invalidate the threshold levels employed in the switching devices.

In regard to the low power operation of our present architecture, it has been argued that the high attenuation rates and low efficiencies associated with present implementations nullify any claim to low power operation. Such an argument confuses the means with the end. Our present implementation serves as a "proof of concept" and verifies the same physical principles as a highly efficient implementation would provide. To provide an analogy, a large fraction of the design strategies employed within modern computers were first employed within vacuum tube or relay based designs (or even Babbage's mechanical units). The fact that such schemes were first proven upon incredibly primitive, unreliable, and inefficient machines does not detract in the slightest from their present merit or utility.

The final argument relative to the validity of the WPD method and our present architecture is as follows: Even with perfect efficiency, the WPD model does not account for the photons which are discarded, and thus not accounted for as mediating photons. We shall now address these arguments.

It is important to note that the photons discarded within one operation carry the result of the same operation performed upon the complement of the input data. As such, this signal may often be put to good use. As an example, the l and d functions employed within our previous report[1] have this relationship and may be implemented simultaneously without the need to discard any light at all. Similar designs may be employed within other applications in order to minimize the quantity of light which is discarded. Unfortunately, this merely leads to an unbalanced signal arriving at the complementary outputs, forcing one of the outputs to sink the previously discarded light.

Given that WPD capable analog operations do not encounter the discarded light problem[2] it is reasonable to assume that problem of discarded light arises within our present architecture as a result of the use of amplitude encoded logic. For this reason it may be possible to address the problem of discarded light by employing some form of phase encoded logic.

The presence of discarded light implies that although each switching device expends a maximum energy of E_{op} per equivalent dyadic logical operation, the net energy expended by the system may be much higher. We argue that it is the energy expended by the switching device that is important. It is the heat dissipation generated by the energy which is consumed by the switching elements within a computer which limits its ultimate speed. For this reason, it is the energy consumed by the switching element which is the limit that is significant.

5. Conclusion

Within the present report we have attempted to model the operation of a HOPLA architecture implementing the multiread function. We have examined how diffraction effects dictate the various limits to the design and fabrication of our system.

We have also considered the power consumption of our architecture. We have shown that in low power operation, when shot noise predominates, that the power consumption of our system is of a significantly low level. We have seen that Caulfield's WPD model of low power operation accounts for such effects, and that successful low power operation of our system should verify aspects of this model.

References

1. H.J. Caulfield and S.A. Kupiec, "A/GATECH DOSP Fabrication", Rome Laboratory Technical Report RL-TR-93-224, (1993)
2. H.J. Caulfield and J. Shamir, "Wave Particle Duality Considerations in Optical Computing", *Appl. Opt.*, Vol. 28, pp. 2184-2186, (1989)
3. H.Jeon, J.Shamir, R.B. Johnson, H.J. Caulfield, J. Kinser, C. Hester and M. Temmen, "The Use of Fixed Holograms for Massively-Interconnected, Low-Power Neural Networks", from *Neural Networks for Human and Machine Perception*, Academic Press, Orlando.
4. J.Shamir, H.J. Caulfield and R.B. Johnson, "Massive Holographic Interconnections and their Limitations", *Appl. Opt.*, Vol. 28, pp 311-324, (1989)

5. J. Gaskill, *Linear Systems, Fourier Transforms, and Optics*, John Wiley & Sons, New York, (1978)
6. J.A. Davis and J.M. Waas, "Current Status of the Magneto-Optic Spatial Light Modulator", Proc. SPIE v.1150, (1989)
7. M.Born and E. Wolf, *Principles of Optics*, Sixth Edition, Pergamon press, Oxford, (1980)
8. A.R. Butz, "Convergence with Hilbert's Space Filling Curves", J. of Computer and Systems Sciences Vol. 3, pp. 128-146, (1969)
9. R.J. Stevens, A.F. Lehar and F.H. Preston, "Manipulation and Presentation of Multidimensional Image Data Using the Peano Scan", IEEE Trans. on Pat. Anal. and Mach. Intel. Vol. PAMI-5, pp. 520-526, (1983)
10. R.Gagliari and S. Karp, *Optical Communications*, John Wiley & Sons, New York, (1976)
11. J.W. Goodman, *Statistical Optics*, John Wiley & Sons, New York, (1985)
12. L.I. Schiff, *Quantum Mechanics*, McGraw Hill, New York, (1949)
13. L. Szillard, "Über die Entropieverminderung in einen Thermodynamischen System bei Eingriffen Intellegenter Wesen." Z. Phys. Vol. 52, pp. 840-856,(1929)

14. L. Brillouin, *Science and Information Theory*, Academic Press, Boston, (1956)
15. R. Landauer, "Irreversibility and Heat Generation in the Computing process", IBM J. Res. Vol. 5, pp 183-191, (1961).
16. E. Fredkin and T. Toffoli, "Conservative Logic", Int. J. Theor. Phys. Vol. 21, pp 219-253, (1982)

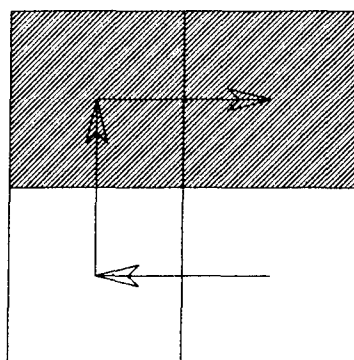
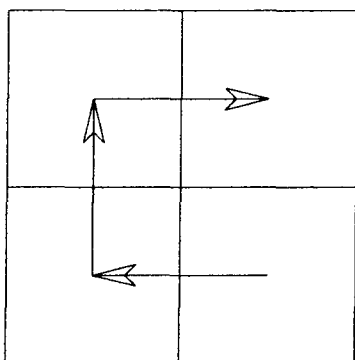
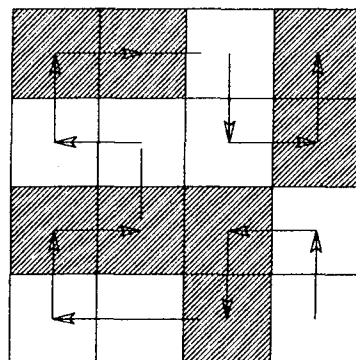
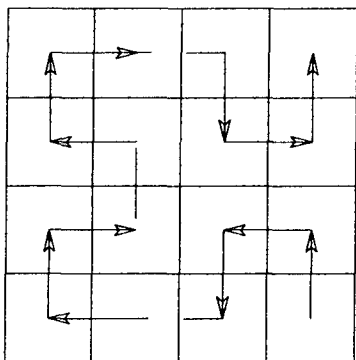
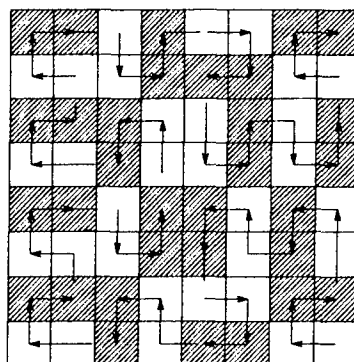
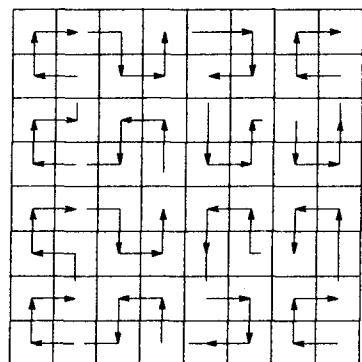
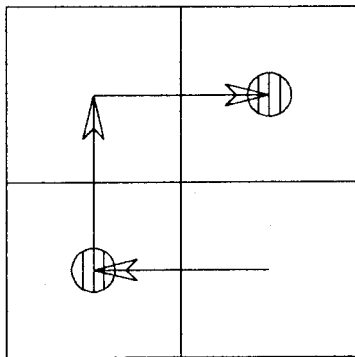
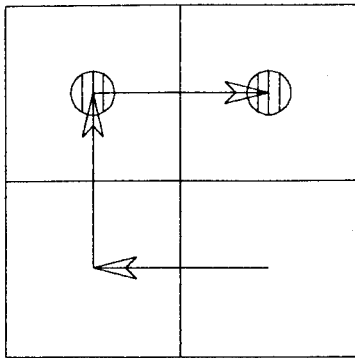
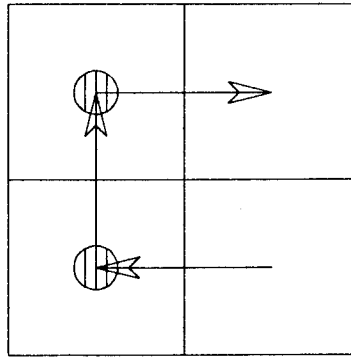
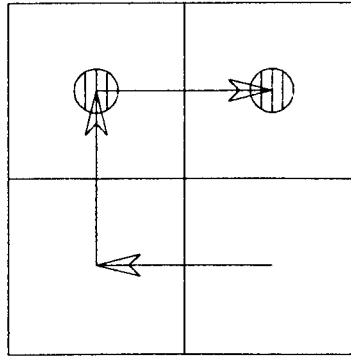


Figure 1



Hilbert Order



Hilbert Order, Grey Coded

Figure 2